Proceedings of the 39th Chinese Control Conference
July 27-29, 2020, Shenyang, China

Flight Control Law Design and Analysis for Mars Airplane in Crosswind

Xin Du, Sheng Zhang

China Aerodynamics Research and Development Center, Mianyang 621000
E-mail: duxin@cardc.cc

Abstract: With the increasing development of Mars detection, Mars airplane as a mesoscale detection means, can be a good complement to fill the ability blank between the track detector and the surface detector. The atmospheric activity on Mars' surface is very intense. However, the current flight control law design for Mars airplane does not consider the effect of crosswind. In this paper, the nonlinear model of Mars airplane, in presence of crosswind, is introduced. Then, the methodology for designing the longitude and lateral controllers is developed. Flight control system in crosswind is designed using the following strategy: when there is a crosswind, control system manipulates the fuselage to turn a yaw angle towards the crosswind direction, and to counter the equivalent sideslip angle caused by the crosswind to ensure that the ground speed direction remains unchanged. The PID control law is used to eliminate errors, and the corresponding angular velocity is introduced to increase damping. Simulation results are obtained using SIMULINK, the results indicate that the control laws proposed in this paper for Mars airplane flying in crosswind are valid and robust.

Key Words: Mars airplane, Crosswind effect, Equivalent sideslip angle, Flight control system, PID controller

1 Introduction

Mars explortion using Mars airplane is a very challenging but also very valuable task. In Mars 2020 mission, a small UAV will be sent along with the Mars rover to the Mars surface, and become the first UAV flying on the surface of extraterrestrial objects[1]. In the foreseeable future, more and more countries will send their own UAVs to the Mars surface, including China. So, flight control of Mars airplane become a critical work for Mars exploration.

For a Mars airplane, Hjartarson presented a blend of H_∞ and proportional–integral controller to stabilize the aircraft under complicated flight conditions[2]. Similarly, Bhattacharya et al. provided the framework of the general mixed sensitivity H_∞ control to solve the longitudinal reference tracking problem, and the results showed that the designed controller can tolerate a potential 70% plant uncertainty[3]. Brown et al. dealt with the work on the design, construction, and flight testing of a Mars airplane demonstrator to show the system stability, control, and performance of the proposed Mars airplane[4]. Y b Liu uses the composite nonlinear feedback technique to design a novel flight control law for a Mars airplane[5]. In domestic, H T Guan developed a robust variable gain controller for Mars airplane based on polytopic linear parameter varying system[6]. S J Han developed an adaptive controller based on compound anti-saturation strategy[7].

None of the above work takes into account the effects of crosswind. In fact, wind on Mars surface is very wild. Large crosswind will change the flight route and cause the failure of the exploration mission. So, flight control law design and analysis for Mars airplane in crosswind is very important. In this paper, the nonlinear model of Mars airplane, in presence of crosswind, is introduced. Then, the methodology for designing the longitude and lateral controllers is developed. At last, simulation results of the performance of the proposed control laws in crosswind are presented and analyzed. Simulation results indicate that the proposed control laws are valid.

2 Problem Statement

This section contains the nonlinear dynamic model of a Mars airplane flying on Mars surface in presence of crosswind. The 6DOF equations of motion is provided by the aerospace blockset of SIMULINK.

2.1 Mars Surface and Atmosphere Model

The Mars atmosphere model used here is a simple curve-fit empirical model of the temperature T, pressure P, density ρ, and speed of sound on Mars a. This model depends on altitude h, and is derived from Mars Global Surveyor data from 1996 and is described by the following equations[2,8]:

$$T = 249.75 - 0.00222h \tag{1}$$

where h is in meters and T is in degree Kelvin.

$$a = \sqrt{\gamma_m R_m T} \tag{2}$$

where $\gamma_m = 1.29$, $R_m = 191.8\left(Nm/kg \bullet K\right)$ and α is in m/s.

$$P = 699e^{-0.00009h} \tag{3}$$

where P is in Pascals.

$$\rho = \frac{P}{R_m T} \tag{4}$$

where ρ is in (kg/m^3).

The acceleration due to gravity is assumed 37.6% of the gravity on earth, $g = 3.69m/s^2$.

2.2 Mars Airplane Model

Mars airplane in this paper is the AERS platform, and autonomous powered airplane developed by NASA. The ARES UAV is pictured in Fig. 1.

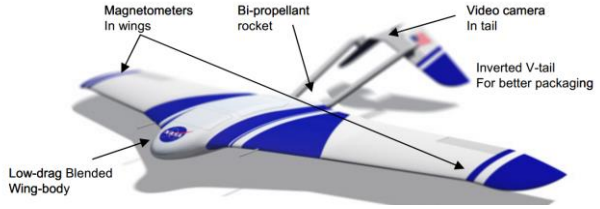

Fig. 1: The ARES vehicle configuration[1]

The mass properties of ARES were given as follows:

Table 1: Mass Properties of ARES

Mass (kg)	100
I_{xx} (kg·m^2)	270
I_{yy} (kg·m^2)	190
I_{zz} (kg·m^2)	460
I_{xy} (kg·m^2)	0
I_{xz} (kg·m^2)	0
I_{yz} (kg·m^2)	0

The wing span of ARES b =6.25m, average cord length $\bar{c}$ =1.25m, surface area S =7.00m^2.

The aerodynamic model of ARES is supplied by lookup tables to derive the various coefficients. These coefficients are used to calculate the aerodynamic forces and moments acting on the airplane.

$$\begin{cases} C_L = C_{L0} + C_L^{\alpha}\alpha + C_L^{\delta_e}\delta_e \\ C_D = C_{D0} + C_D^{\alpha}\alpha + C_D^{\delta_e}\delta_e + C_D^{\beta}\beta + C_D^{\delta_r}\delta_r + C_D^{\delta_a}\delta_a \\ C_Y = C_Y^{\beta}\beta + C_Y^{\delta_r}\delta_r \\ C_l = C_l^{\beta}\beta + C_l^{\delta_r}\delta_r + C_l^{\delta_a}\delta_a + \dfrac{\left(C_l^{p}p + C_l^{r}r\right)b}{2V} \\ C_m = C_{m0} + C_m^{\alpha}\alpha + C_m^{\delta_e}\delta_e + \dfrac{\left(C_m^{\dot{\alpha}}p + C_m^{q}q\right)\bar{c}}{2V} \\ C_n = C_n^{\beta}\beta + C_n^{\delta_r}\delta_r + C_n^{\delta_a}\delta_a + \dfrac{\left(C_n^{p}p + C_n^{r}r\right)b}{2V} \end{cases} \quad (5)$$

where C_L , C_D , C_Y , C_l , C_m , C_n are coefficient of lift, coefficient of drag, coefficient of side force, coefficient of rolling moment, coefficient of pitching moment, and coefficient of yawing moment respectively, δ_e is the elevator deflection angle, δ_a is aileron deflection angle, δ_r is rudder deflection angle, p is rolling rate, q is pitching rate, r is yawing rate, V is vehicle velocity. Maximum deflection angles of actuators are set to be[1]

$$\begin{cases} -20\,\text{deg} \le \delta_e \le 20\,\text{deg} \\ -20\,\text{deg} \le \delta_a \le 20\,\text{deg} \\ -20\,\text{deg} \le \delta_r \le 20\,\text{deg} \end{cases} \quad (6)$$

To input to the engine is a normalized thrust command δ_T , (scaled between 0 and 1), and the thrust is modeled simplely by[1]

$$T = T_{scale} \bullet \delta_T \quad (7)$$

where T_{scale} =250N.

2.3 Crosswind Model

The 6DOF (Euler Angles) block considers the rotation of a body-fixed coordinate frame (X_b, Y_b, Z_b) about a flat Mars reference frame (X_e, Y_e, Z_e). The origin of the body-fixed coordinate frame is the center of gravity of the body, and the body is assumed to be rigid, an assumption that eliminates the need to consider the forces acting between individual elements of mass. The flat Mars reference frame is considered inertial, an excellent approximation that allows the forces due to the Mars's motion relative to the "fixed stars" to be neglected.

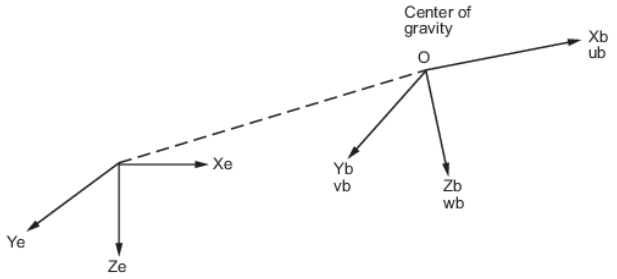

Fig. 2: Flat Mars reference frame and body-fixed coordinate frame

Crosswind is modeled in flat Mars reference frame, whose velocity is assumed to be

$$\vec{V}_{we} = 0\vec{i}_e + V_w\vec{j}_e + 0\vec{k}_e \quad (8)$$

where $\vec{i}_e$, $\vec{j}_e$, $\vec{k}_e$ are the three unit vectors of body-fixed axes.

The coordinate transformation matrix from flat Earth axes to body-fixed axes is assumed to be M_{eb} . So the crosswind velocity in body-fixed coordinate frame is

$$\vec{V}_{wb} = M_{eb}\vec{V}_{we} \quad (9)$$

The ground speed of airplane is assumed to be $\vec{V}_d$, the airplane velocity vias air is assumed to be $\vec{V}_a$. In body-fixed frame, $\vec{V}_a$ can be calculated as follows:

$$\vec{V}_a = \vec{V}_d + \vec{V}_{wb} = V_{ib}\vec{i}_b + V_{jb}\vec{j}_b + V_{kb}\vec{k}_b \quad (10)$$

where $\vec{i}_b$, $\vec{j}_b$, $\vec{k}_b$ indicates the three sss of body-fixed axes. The angle of attack and the sideslip angle are obtained by

$$\alpha = \tan^{-1}\left(\frac{V_{kb}}{V_{ib}}\right) \quad (11)$$

$$\beta = \sin^{-1}\left(\frac{V_{jb}}{\sqrt{V_{ib}^2 + V_{jb}^2 + V_{kb}^2}}\right) \quad (12)$$

3 Flight Control Law Design

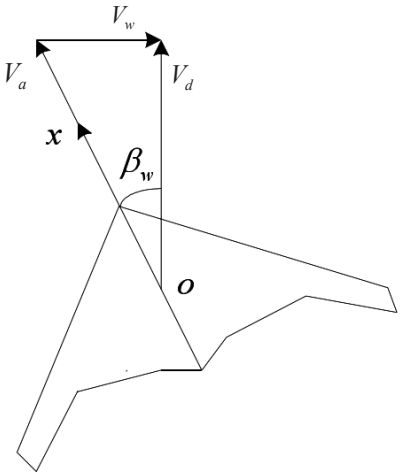

Fig. 3: The Mars airplane in presence of crosswind

As seen in Fig. 3, crosswind will cause an equivalent sideslip angle β_w:

$$\beta_w = \tan^{-1}\left(\frac{|\vec{V}_w|}{|\vec{V}_d|}\right) \tag{13}$$

If no crosswind control system is available, the lateral deviation of route y will increase rapidly, as seen in Fig. 4.

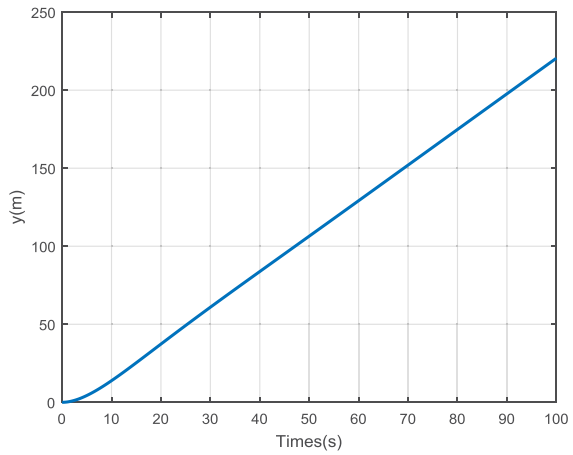

Fig. 4: Lateral deviation without crosswind control system

In this paper, flight control system in crosswind is designed using the following strategy: when there is a crosswind, control system manipulates the fuselage to turn a yaw angle $\psi=\beta_w$ towards the crosswind direction, and to counter the equivalent sideslip angle caused by the crosswind to ensure that the ground speed direction remains unchanged[9-10].

A PI control law is used to stablize velocty:

$$\delta_T = \left(K_V + \frac{K_{iV}}{s}\right)\frac{V - V_{cmd}}{V_{cmd}} \tag{14}$$

A PID control law is used to stablize altitude:

$$\delta_e = \left(K_h + \frac{K_{ih}}{s}\right)(h - h_{cmd}) + K_{dh}\dot{h} + K_q q + K_\theta \theta + K_\phi \phi \tag{15}$$

where θ is pitch angle, ϕ is roll angle. When the airplane turns, the altitude will decrease if there is no elevator change. So roll angle is introduced here as a feedback term.

A PID control law is used to stablize lateral deviation:

$$\delta_a = \left(K_y + \frac{K_{iy}}{s}\right)(y - y_{cmd}) + K_{dy}V_y + K_p p + K_\phi \phi \tag{16}$$

where V_y is the velocity along the Y-axes of flat Mars reference frame.

Sideslip angle is controlled to 0 in this case, so control law for rudder is as follows:

$$\delta_r = K_\beta \beta + K_r r \tag{17}$$

All control laws are constructed in SIMULINK, the lateral deviation stabilizer is shown in Fig. 6.

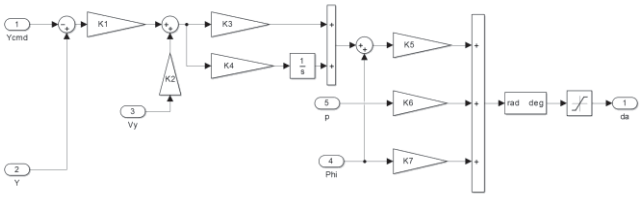

Fig. 5: Control structure of y stabilizer

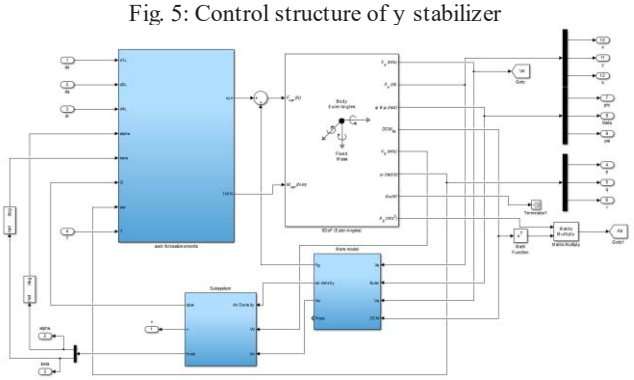

Fig. 6: 6DOF motion simulation frame

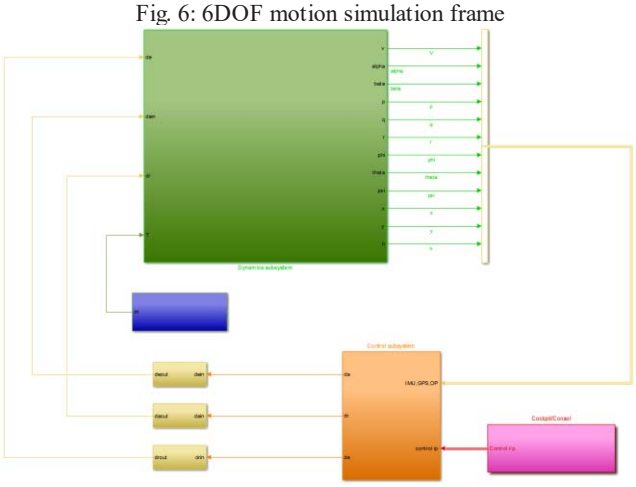

Fig. 7: Flight control system frame

The 6ODF motion simulation frame is shown in Fig. 6, and the whole flight control system frame is shown in Fig. 7.

4 Illustrative Example

Using the least-squares fitting methods for these aerodynamic coefficients of ARES in [3], the resulting aerodynamic expressions are approximately obtained by[5].

$$\begin{cases} C_L = 5.0512\alpha + 0.2346 \\ C_D = 2.3114\alpha^2 - 0.0096\alpha + 0.0364 \\ C_Y = -0.2578\beta \\ C_l = 0.0688\beta - 0.1490\delta_a \\ C_m = 1.9091\alpha^2 - 0.5638\alpha + 0.0401 - 0.8595\delta_e \\ C_n = 0.0859\beta - 0.0802\delta_r \end{cases} \tag{14}$$

The initial altitude $h_0 = 2500m$, initial velocity $V_0 = 150m/s$. The velocity of crosswind is set to be 25m/s. So, the equivalent sideslip angle caused by crosswind is $\beta_w = 9.46°$. Flight control system need to control β to a steady state of $0°$, and control ψ to a steady state of $9.46°$. Simulation results are shown in Fig. 8-17.

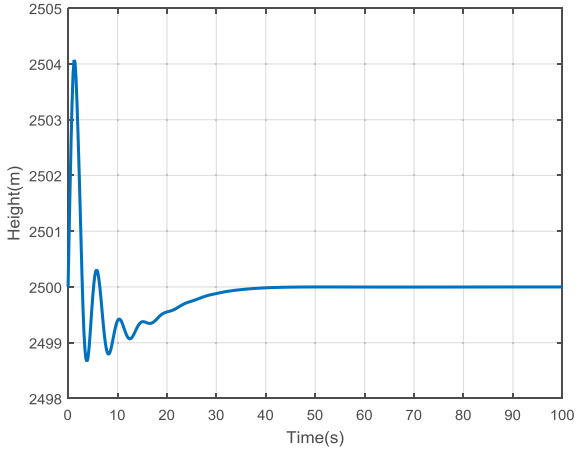

Fig. 8: Altitude curve

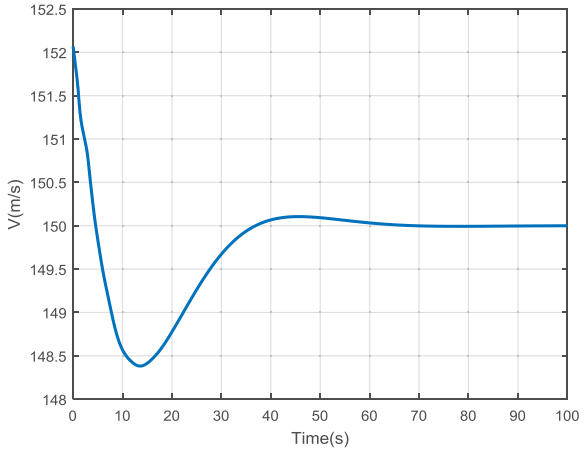

Fig. 9: Velocity curve

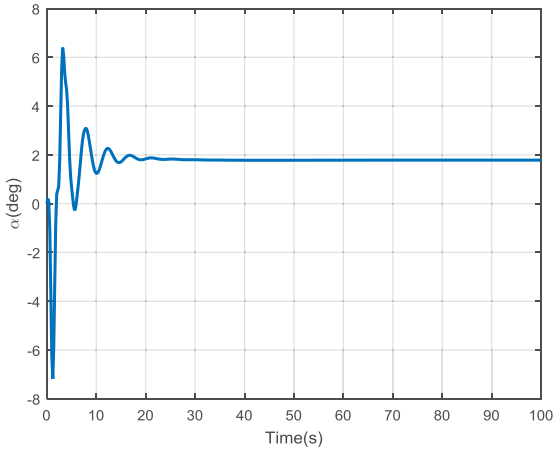

Fig. 10: Angle of attack curve

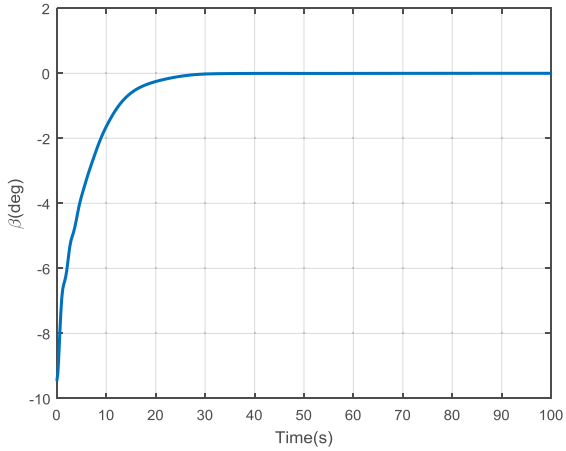

Fig. 11: Sideslip angle curve

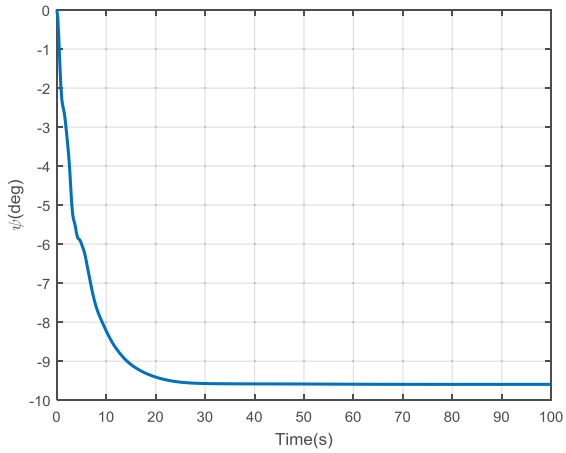

Fig. 12: Yaw angle curve

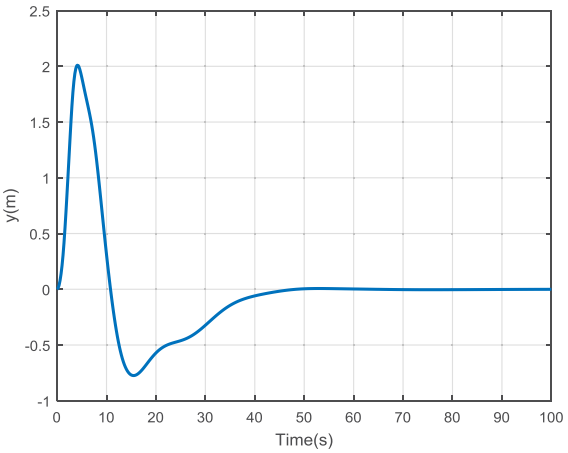

Fig. 13: Lateral deviation curve

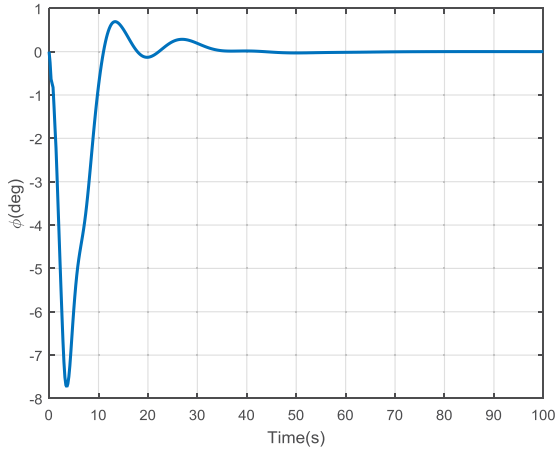

Fig. 14: Roll angle curve

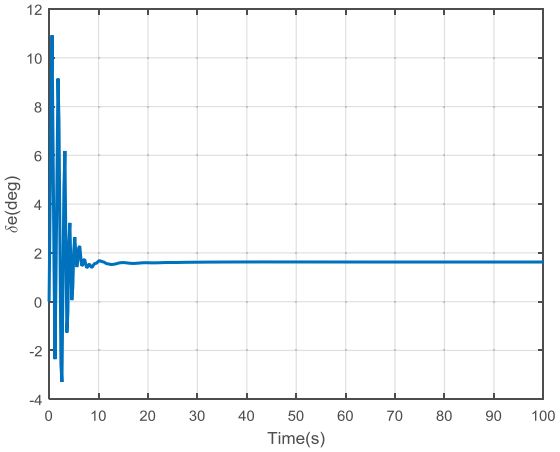

Fig. 15: Elevator curve

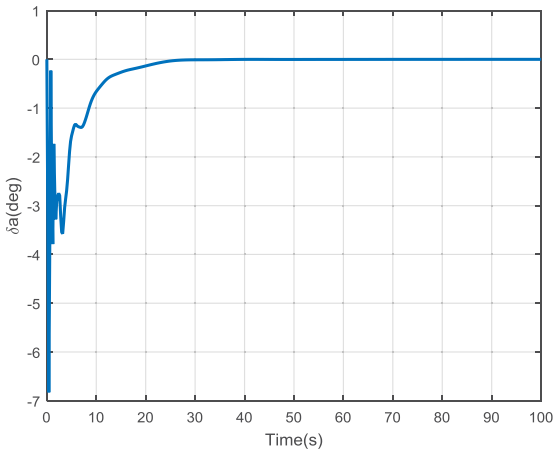

Fig. 16: Aileron curve

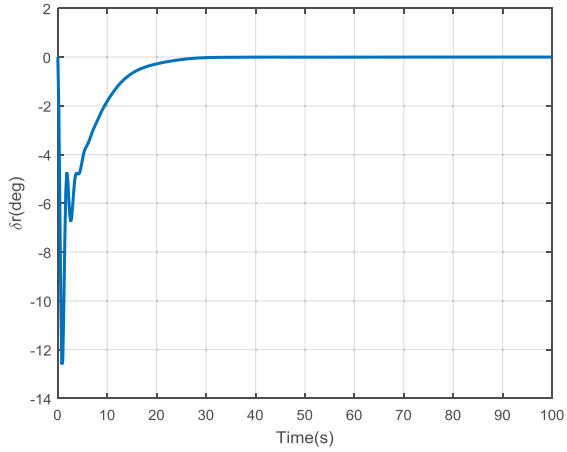

Fig. 17: Rudder curve

Fig. 8-10 gives the results of longtitude control. Altitude change is no greater than 5m, and velocity change is no greater than 2m/s. Altitude and speed converge around the time of 50 seconds.

As seen in Fig. 11 and Fig. 12, β is controlled to a steady state of 0°, and ψ is controlled to a steady state of 9.46°. This is consistent with the previous analysis conclusions. Sideslip angle and yaw angle converge around the time of 30 seconds.

As seen in Fig. 13, lateral deviation change is no greater than 2m, Mars airplane's flight route under crosswind is very well maintained. Lateral deviation converge around the time of 50 seconds.

As seen in Fig. 15-17, in crosswind of a velocity 25m/s, the maximum elevator deflection angle is about 12°, the maximum aileron deflection angle is about 7°, and the maximum rudder deflection angle is about 12°. All control inputs do not exceed the maximum available range.

Fig. 18~20 show respectively the altitude, lateral deviation, and velocity curves for 500 cases. The dispersions in the aerodynamic coefficients (C_L, C_D, C_Y, C_l, C_m, C_n) are set to be Gaussian distribution, whose 3σ values are set to be 20%. The simulation results of the 500 cases indicate that the control law has good robustness.

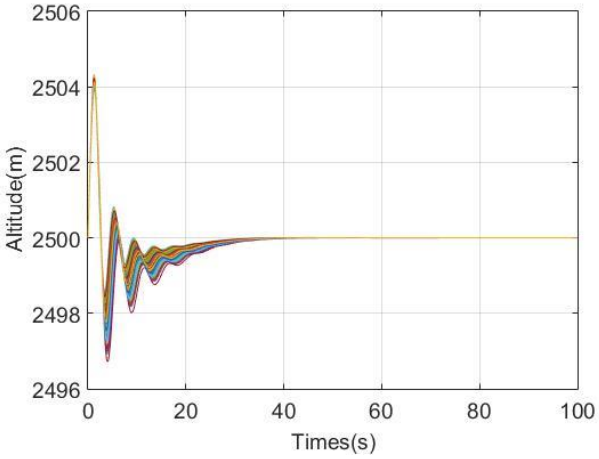

Fig. 18: Altitude curve (500 cases)

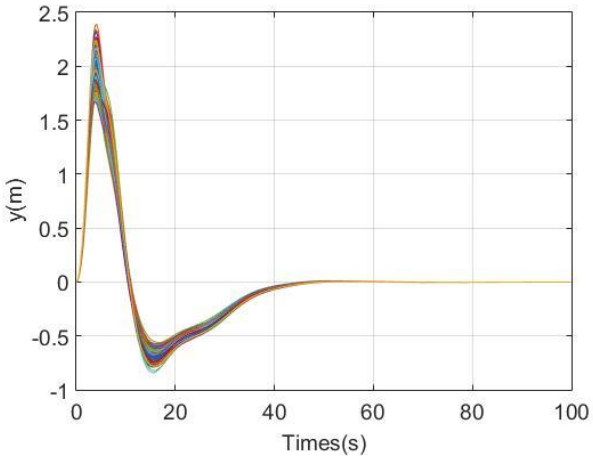

Fig. 19: Lateral deviation curve (500 cases)

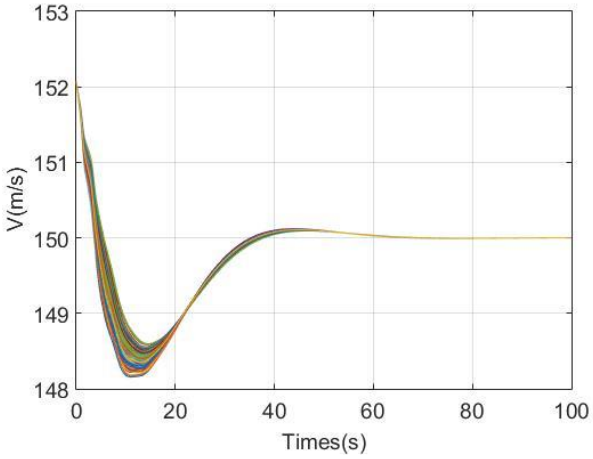

Fig. 20: Velocity curve (500 cases)

4.1 Conclusion

This article designs a flight control system to achieve stable flight of Mars aircraft in crosswind. Crosswind will cause an equivalent sideslip angle, and the flight control system is designed to eliminate the sideslip angle, an to ensure that the ground speed direction remains unchanged. The PID control law is used to eliminate errors, and the corresponding angular velocity is introduced to increase damping. Simulation results indicate that the control laws proposed are valid and robust.

References

[1] https://mars.nasa.gov/mars2020/.

[2] Hjartarson A., Paw Y C., and Chakraborty A., Modeling and Control Design for the ARES Aircraft, *AIAA Guidance, Navigation and Control Conference and Exhibit*, AIAA paper 2008-7452.

[3] Bhattacharya R., and Valasek J., On Modeling and Robust Control of ARES, *AIAA Guidance, Navigation and Control Conference and Exhibit*, AIAA paper 2008-7454.

[4] Brown N., Samuel A., and Colgren R., Mars Exploration Airplane Design, Construction, and Flight Testing of a Stability, Control and Performance Demonstrator, *AIAA Infotech@Aerospace Conference and Exhibit*, AIAA paper 2007-2723.

[5] Y B Liu., K M Peng., Y P Lu., B M Chen., Flight Control Law Using Composite Nonlinear Feedback Technique for a Mars Airplane, *Journal of Guidance, Control, and Dynamics*. 2016, 39(9): 2194-2202.

[6] H T Guan., Y C Zhao., K Ni., Q Z Zhang., Robust Variable Gain Control for Mars Airplane Based on Polytopic LPV, *Missiles and Space Vehicles*, 2018, 1: 69-74. (In Chinese)

[7] S J Han., K Ni., C P Xiong., Q Z Zhang., Adaptive Control of Mars Aircraft Based on Compound Anti-Saturation Strategy, Aerospace Control, 2017, 35(3): 40-48. (In Chinese)

[8] Restrepo C., and Valasek J., Structured Adaptive Model Inversion Controller for Mars Atmospheric Flight, *Journal of Guidance, Control, and Dynamics*, 2008, 31(4): 937-953.

[9] James M B., Tailless Aircraft Control Allocation, *AIAA Guidance, Navigation, and Control Conference*, AIAA paper 1997: 737-747.

[10] James M B., Andrew G S., and David B.L., Synthesis and Analysis of DynamicInversion and LPV Tailless Flight Control Law Designs, *AIAA Guidance, Navigation, and Control Conference and Exhibit*,, AIAA paper 1998: 900-908.